International Journal of Environmental Science and Technology
https://doi.org/10.1007/s13762-021-03382-3

ORIGINAL PAPER

Formation of improved activated carbons from sugarcane bagasse as environmental materials for adsorption of phenolic pollutants

K. M. S. Khalil[1] · M. Khairy[1] · O. A. S. Allam[1,2] · M. K. Khalil[3]

Received: 21 November 2020 / Revised: 31 March 2021 / Accepted: 7 May 2021

Abstract

Phenolic pollutants are very toxic and their removal from aquatic resources is very important. Adsorption by activated carbon, AC, is the best method for removal of phenols from solutions. However, the high cost of AC and difficulty of its regeneration after phenol adsorption puts high demand on low price AC materials. Therefore, sugarcane bagasse as a sustainable, bulky and fibrous biomass was selected for the purpose of low-price AC formation for phenols adsorption. Sugarcane bagasse derived activated carbon, BAC, was achieved via an environmental thermo-chemical activation process using $ZnCl_2$ followed by pyrolysis at different temperatures (400–600 °C). The formed BAC materials were characterized by elemental analysis, simultaneous TGA–DTA, ATR-FTIR, XRD, Raman spectroscopy, SEM, and nitrogen adsorption/desorption techniques. The BAC materials showed several enhanced characteristics including extra high specific surface area (up to 2046 m^2/g), improved meso-/microporosity dual system and nanostructured graphitic-like structure composed of few graphene layers. Adsorption removal of phenol as an industrial waste pollutant was investigated from solutions of wide range of concentrations (50–1000 mg/L). The adsorption processes were characterized by (L2) class of adsorption isotherm, Langmuir isotherm model, physical-adsorption thermochemical parameters and pseudo-second-order kinetics. Adsorptions of two other substituted phenols (resorcinol and pyrogallol) were investigated. The adsorption capacity was increased with increasing of intramolecular bonding of the adsorbate in the order of phenol < resorcinol < pyrogallol. The present results emphasized the versatility of the formed BACs as environmentally sustainable adsorbent for phenolic pollutants.

Keywords Activated carbon · Environment · Graphene layers · Contaminates · Pollutants

Introduction

Phenolic compounds belong to the group of common environmental contaminants produced in industrial effluents, which are very toxic and classified as priority pollutants (Priya and Sureshkumar 2020; Villegas et al, 2016; Girods et al. 2009; Dabrowski et al. 2005). The main industrial sources of phenols/phenolic compounds emission are discharged from manufacturing of pesticides, chemicals, pharmaceuticals, paper, wood, petroleum refining, and olive oil extraction units (Girods et al. 2009; Michailof et al. 2008).

In fact, phenols are not bio-degradable compounds, although the permissible concentration level of phenols in drinking water is about 1.0 µg/L according to the World Health Organization (WHO). Phenols/phenolic compounds are highly soluble in water; therefore, their presence leads to serious contamination of drinking water resources that causing unpleasant odor. Contamination with phenols lead to harmful effects to aquatic flora, fauna, aquatic organisms and prevent the regular acts of biological community (Hameed and Rahman 2008; Al-Malack and Dauda 2017; Lorenc-Grabowska et al. 2016). Phenol contamination may cause serious health problems that can be acute and chronic. Thus, from the medical point of view, phenols contamination may cause intensive risk to human kind health, such as kidney and liver damage, protein degeneration, tissue erosion, sour mouth, diarrhea, impaired

Editorial responsibility: Binbin Huang.

✉ K. M. S. Khalil
kms_khalil@yahoo.co.uk

[1] Chemistry Department, Faculty of Science, Sohag University, Sohag 82524, Egypt

[2] Agricultural Research Center, ARC, Ministry of Agriculture, Giza, Egypt

[3] Faculty of Medicine, Sohag University, Sohag 82524, Egypt

Published online: 31 May 2021

vision and paralysis of the central nervous system (Karri et al. 2017a; Kumar and Jena 2016). Long-term exposure can lead to irregular breathing, muscle weakness, tremor, coma, and respiratory arrest at lethal doses in humans, irritation of the skin, eyes, and mucous membranes (Villegas et al. 2016). Therefore, it is necessary to eliminate phenol from aquatic resources to prevent its harmful impacts on water, streams and human life (Velasco et al. 2014; Yagmur et al. 2017).

Adsorption is the best and most frequently employed method for removal of phenols from solutions. Activated carbon (AC) possesses perfect adsorption ability for relatively low-molecular-weight organic compounds such as phenols and benzene derivatives (Dabrowski et al. 2005; Derylo-marczewska et al. 2011). Adsorption by AC is a method that currently applied in water plants as tertiary treatment for pollutants removal (Bernal et al. 2020). It has been established that surface properties of AC adsorbent depend on the presence of heteroatoms (such as oxygen or nitrogen) that determine the type of charge, surface hydrophobicity, and electronic density of the AC graphene layers. However, the entire adsorption process of phenols affected by both of surface chemistry of AC adsorbent and its nanoporous porous texture (Derylo-marczewska et al. 2011).

However, the application of AC materials as adsorbents for phenols adsorption is limited by its high cost and the irreversible nature of phenols adsorption process that prevent the AC regeneration. In fact, adsorption of phenols from solution occurs via physisorption but physically adsorbed phenols become irreversibly chemisorbed in the course of time and/or by increasing the temperature. Therefore, AC adsorbents cannot be regenerated (Magne and Walker 1986). Thus, different thermo-chemical methods have been investigated for the conversion of biomass of agricultural residues, as renewable and non-expensive starting materials for AC adsorbents formation (Açıkyıldız et al. 2014; Gundogdu et al. 2012; Angin 2014; Khenniche and Benissad-Aissani 2010; Gonçalves et al 2014; Wassie and Srivastava 2016; Karri et al 2017b; Khalil et al. 2017).

Among the different biowaste materials, sugarcane bagasse is a renewable and non-expensive agro-industrial material. Sugarcane bagasse is a massive by-product from sugarcane industry and mainly used as a raw biomass fuel in power plants. However, sugarcane bagasse can offer many more valuable advanced utilization opportunities due to its solid, bulky and fibrous biomass properties (Congsomjit and Areeprasert 2020). Sugarcane bagasse has recently been investigated for the formation of mesoporous structure with high adsorption capacity (Liou 2010); simultaneous production of sugars, graphene quantum dots, and porous carbon (Chai et al. 2019); efficient adsorbents formation and preparation of two-dimensional graphene crystal (Long et al. 2019).

Remarkably, BAC's materials have been investigated as adsorbents for raw sugarcane juice purification (Solís-fuentes et al. 2019); Cr (VI) adsorption (Luo 2019; Karri et al. 2020); tetracycline hydrochloride (Cai et al 2019); naphthalene removal (Eslami et al 2018) and removal of diclofenac sodium (Abo ELNaga et al. 2019).

The present work investigates the utilization of sugarcane bagasse, as a sustainable precursor for the production of nanostructured activated carbon materials with extra-high surface and improved adsorption characteristics. While many phenol adsorption studies have concerned with low phenol concentrations, the present study investigates the adsorption from solution of wide range of concentrations (50–1000 mg/L), which is analogous to concentrations of industrial effluents. Moreover, adsorption of two other related phenols (resorcinol and pyrogallol as dihydroxy and trihydroxy phenols, respectively) was investigated to learn about the adsorption behavior of the BAC materials towards other phenolic compounds. The adsorption process was treated by different adsorption models, kinetic equations and thermodynamic functions to realize the adsorption mechanism. The adsorption capacity of the formed BAC materials is compared with a number of recently investigated materials. This work was carried out at Sohag University, Sohag, Egypt, throughout the last two years.

Materials and methods

Materials

Sugarcane is a very important plant grown in many warm areas all over the world and mainly used for sugar manufacture. In this study, sugarcane grown in Sohag district of Upper Egypt was employed as a precursor for ACs preparation. The bagasse residual material obtained after juice extraction process by a "roll-mills" machine, dried in open-air atmosphere (25–30 °C) and cut into small pieces ≤ 2 cm in length. Phenol, resorcinol and pyrogallol compounds obtained from Biotech Ltd chemicals, 99.5%. Phenols were used as received without any further purification.

Preparation of sugarcane bagasse activated carbons, BACs

In this study, BACs derived from sugarcane bagasse were formed via thermo-chemical activation using $ZnCl_2$ as an activation reagent. Typically, 20.0 g of air-dried sugarcane bagasse portions was weighted and each portion was impregnated in 200 mL of 10% $ZnCl_2$ solution. The impregnated mixtures were heated up to 100 °C in a drying oven for 12 h. Then, the dried mixtures were placed in a crucible and activated in a muffle furnace at 400, 500 or 600 °C (heating

rate of 10 °C/min, hold at final temperature for 1.0 h) in a flow of N_2 gas (150 mL/min). After activation and cooling down, the obtained materials were boiled with 500 mL of HCl (0.50 M) solution and then washed several times with hot and cold distilled water to remove any impurities/residues of $ZnCl_2$. The washed materials were finally dried for 24 h at 120 °C. Thus, the final yield (%) of the obtained ACs was calculated by the following equation:

$$\text{Yield}\,(\%) = \frac{\text{weight of ACs (g)}}{\text{weight of raw bagasse (g)}} \times 100 \quad (1)$$

The formed bagasse derived activated carbon materials produced by $ZnCl_2$ thermochemical activated method at 400, 500 and 600 °C were denoted as BAC400, BAC500 and BAC600, respectively. Where, the term "BAC" refers to bagasse derived activated carbon and the three following digits (400, 500 and 600) refer to the employed activation temperature of each material.

Characterization techniques

Bulk analyses

Elemental analysis, Simultaneous Thermogravimetric-Differentials thermal analysis (TGA -DTA), Fourier transforms Infrared spectroscopy (FTIR), and powderX-ray diffractometry (XRD) were carried out according to the standard methods reported elsewhere (Khalil et al. 2017).

Raman spectroscopy

Raman spectra of the materials were obtained using Raman spectroscopy model SENTERRA, Inverted Configuration (Germany) at ambient condition. A 785 nm laser source was used as an exciting source on the sample surface with a power of 50 mW.

Nitrogen adsorption/desorption isotherms

N_2 adsorption/desorption isotherms of the BACs were measured using ASAP 2010 instrument (Micrometrics Instrument Corporation, U.S.A.) at − 196 °C. Each BAC sample was outgassed prior to gas adsorption measurement at 300 °C under vacuum conditions for 5 h. The specific surface areas were calculated using the BET equation (Brunauer et al 1938). The *t*-plot method was employed, using Halsey equation (Halsey1948), to assess microporosity and calculate external surface area according to the IUPAC regulations (Sing et al 1985). The total pore volume (V_T) was estimated at a relative pressure (p/p_o) = 0.95.

Table 1 The formation yield (%) and the elemental analysis results for the BAC materials obtained at different activation temperatures

Sample	Mass percentages				
	Yield	C	H	N	O
BAC 400	34.8	76.4	1.9	1.1	20.6
BAC500	30.7	77.9	1.5	0.4	20.2
BAC600	27.3	85.1	1.1	0.0	13.8

Scanning electron microscopy (SEM)

SEM micrographs were obtained by using a JEOL-JSM-5400LV scanning electron microscope. The samples were coated with a thin gold layer prior to investigation.

Phenol adsorption experiments

The adsorption capacity of phenol on the prepared BACs was performed following a procedure similar to that employed by Girods et al. (Dabrowski et al. 2005). Typically, portions of an accurate mass of 0.100 g of each BAC material were added to a group of flasks (50 mL in volume), each containing 25.0 mL of aqueous phenol solutions with an initial concentration in the range of 100–600 mg/L. Due to the fact that the entry of oxygen is known to lead to irreversible phenol adsorption through oxidative coupling, the solution flasks were hermetically well closed to avoid the loss of phenol by volatilization and minimize the exposure to air oxygen. The flasks were then placed in a thermostatic atmosphere adjusted at 25 (± 1) °C and stirred over a period of 24 h to assure reaching of equilibrium, which was found to be attained after ~ 5 h. The equilibrium concentration of phenol was measured by a double beam UV–Vis spectrophotometer model (Pg T80) at 269 nm.

The kinetic studies were carried out by adding 0.100 g portion of the BAC materials in 50 mL of phenol with initial concentration of (50–400 mg/L) and then stirred for several time intervals. Adsorption quantity, q_e (mg/g), was calculated by using the equation of $q_e = (C_o - C_e)\ V/m$, where C_o and C_e are the initial and equilibrium concentrations, respectively. V is the volume of the solution and m is the BAC mass, respectively.

Results and discussion

Characterization of activated carbons

Chemical composition and yield (%)

The formation yield (%) and elemental analysis results for the BAC materials obtained at different activation

temperatures are cited in Table 1. Thus, yield (%) values were amounting to 34.8, 30.7 and 27.3%, for BAC400, AC500 and AC600, respectively. This decreasing order was explained in terms of evolution of more volatile and/or carbon species with increasing of the activation temperature (Hazzaa and Hussein 2015; Rambabu et al. 2014). Elemental analysis results showed that carbon content was increased (from 76.4, 77.9 to 85.1%) for BAC400, BAC500 and BAC600, respectively. However, elemental contents of other elements were decreased as: H (1.9, 1.5 to 1.1%); N (1.1, 0.4 to 0.0%); O (20.6, 20.2 to 13.8%) for BAC400, BAC500 and BAC600, respectively.

TGA–DTG and DTA curves for BAC400, BAC500 and BAC600 in a flow of air are shown in Fig. 1a, b, respectively. Single weight loss step was observed, with a DTG peak maximized at 513, 530 and 555 °C for BAC400, BAC500 and BAC600, respectively. The observed weight loss was due to combustion process, which was confirmed by an exothermic peak at the same temperature on the combined DTA curve of BAC400. This result indicated that thermal stability of the formed materials was increased with increasing of the activation temperatures. Moreover, combustion residues at 900 °C (calculated from the TGA curves) were amounting to just 2.60 for BAC400 and drops to 0.85% for BAC600. This indicates low ash contents in the present materials, which is due to the effect of the employed method in decreasing of ash residue. This effect was increased with increasing of the activation temperature.

FTIR spectroscopy

FTIR spectra of the formed materials BAC400, BAC500 and BAC600 are shown in Fig. 2a. The observed bands were interpreted in light of the standard FTIR tables (Coates 2000) and spectra reported for similar materials (Liou 2010; Yang and Qiu 2010; Yang and Lua 2006) as follows. The band observed at 3360 cm^{-1} was attributed to the presence of ν(O–H). The bands observed in the region 1700–1500 cm^{-1} were attributed to *stretching mode of* some different C=O, C=C groups, as indicated in Table 2. The band observed at 1150 cm^{-1} was attributed to the presence of ν (C–O) stretching vibrations which may present in acids, alcohols, phenols, ethers and/or ester. The band observed around 880 cm^{-1} was attributed to bending vibration of δ (C–H). The band observed at 453 cm^{-1} was related δ (C–O) and (C–C). The small band at 1690 cm^{-1} was ascribed to ν (C=O) for ketones, aldehydes or carboxyl's groups, (Adinaveen et al. 2013) which, indicates that the BAC carbons contain a small amount of carboxyl group. Thus, FTIR spectra suggested the development of highly aromatic activated carbon structure with small amount of carbonyl, ketone, carboxylic anhydride, alcohols, phenols, ethers and/or ester groups.

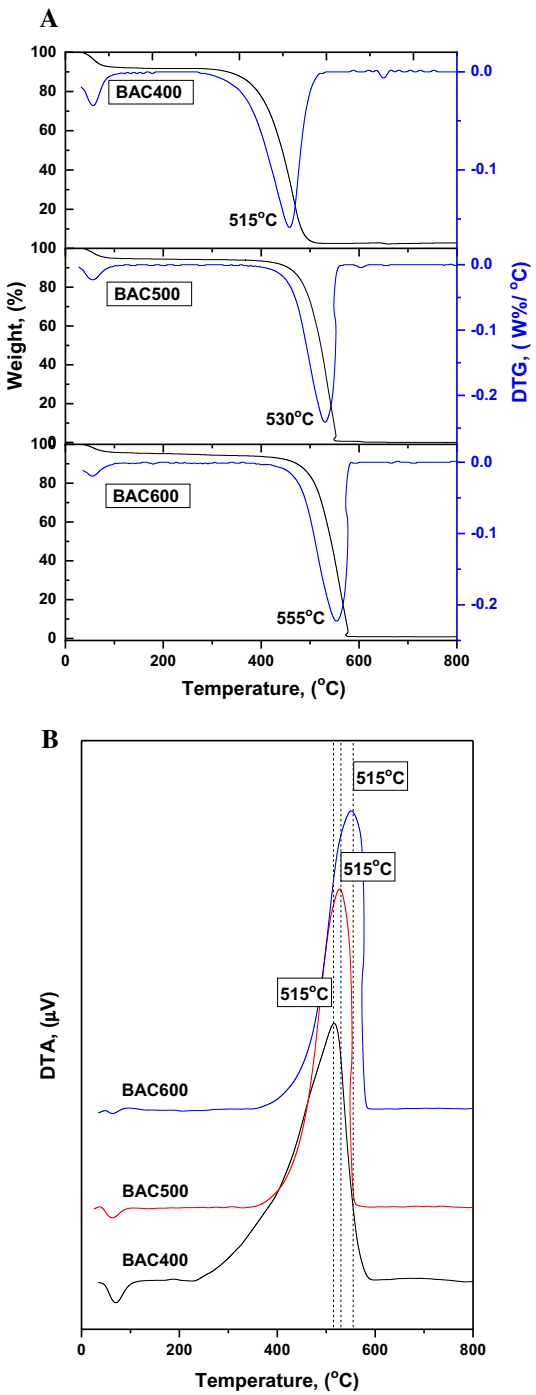

Fig. 1 TG–DTG curves (**a**) and the simultaneous DTA curves (**b**) for BAC400, BAC500 and BAC600 materials in a flow of air atmosphere

The effect of increasing of activation temperature on going from BAC400, BAC500, to BAC600 can be realized by further inspection of Fig. 2a. The intensity of the bands attributed to acidic groups (at 1694, 1150 and 453 cm^{-1} related to ν (C=O), ν (C–O) and δ (C–O), respectively) were decreased (Rambabu et al. 2014). Moreover, the band

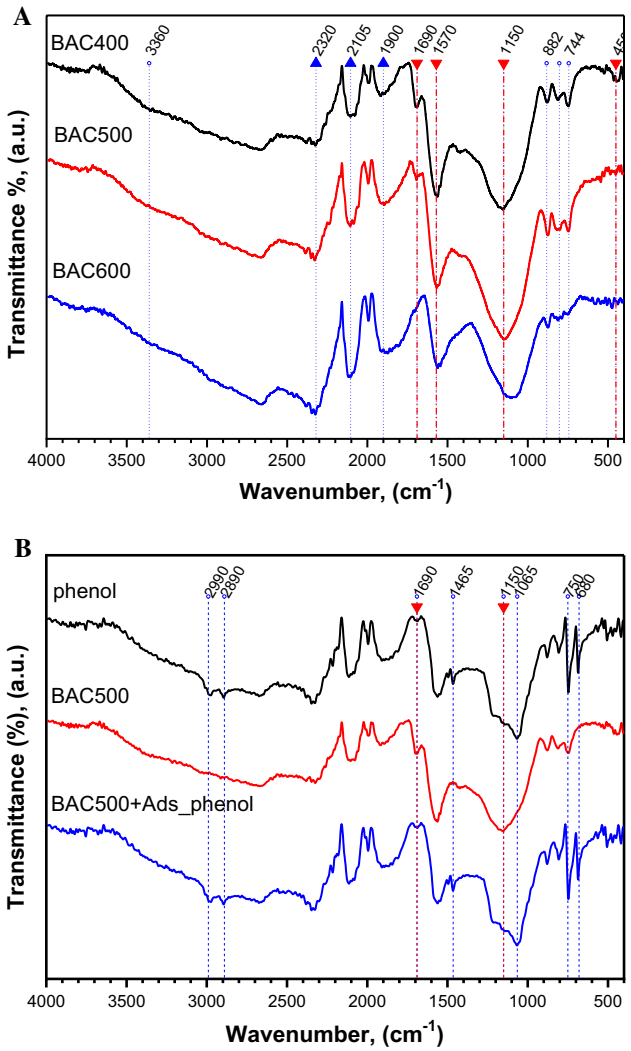

Fig. 2 ATR-FTIR patterns (**a**) for BAC400, BAC500 and BAC600 materials and (**b**) for phenol, BAC500 and "BAC500 with adsorbed phenol"

Table 2 FTIR Bands wavenumbers and their assignment for the formed BAC materials

Band wavenumber, cm^{-1}	Assignment
3360	ν (O–H)
1900	ν (C=O) of five members ring anhydrides
1690	ν (C=O) carboxylic acid
1574	ν (C=C) in aromatic rings
1150	ν (C–O) stretching vibrations in acids, alcohols, phenols, ethers and/or ester groups
882, 803 and 744 cm^{-1}	δ (C–H) out of the plane binding deformation mode of substituted benzene rings
453	δ (C–O) and (C–C) symmetric bending

assigned for ν (C=O) of five members ring anhydrides was largely increased. This suggests increasing of anhydride formation with increasing of activation temperatures. These results indicated that successive removal and dehydration of surface functional groups were occurred with increasing of activation temperature, which was confirmed by XRD results shown below.

XRD diffractometry

XRD patterns for BAC400, BAC500 and BAC600 are shown in Fig. 3. The patterns indicated the formation of graphitic carbon structure, characterized by two broad diffraction peaks at $2\theta \approx 22$ and 44°, which were indexed to the (002) and (100) reflection of graphitic carbon, respectively (File No., 75-1621, JCPDS). The presence of these

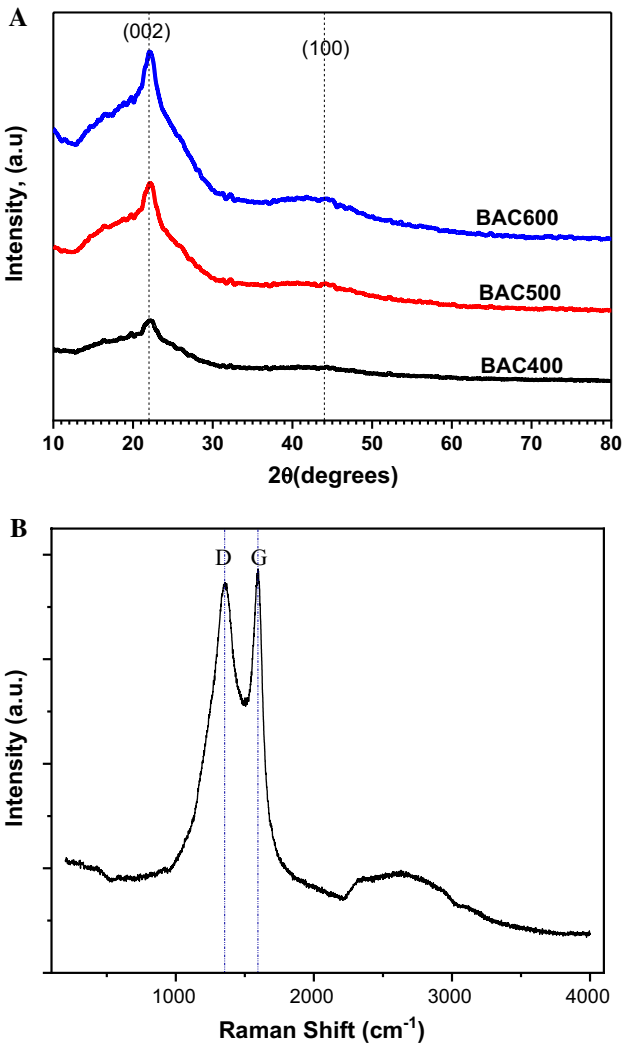

Fig. 3 XRD powder diffractions for BAC400, BAC500 and BAC600 materials (**a**), and Raman spectrum for BAC500 material as an example (**b**)

two broad peaks indicated that the materials were structured in graphite micro-crystallites (Shi et al. 2016) composed of few graphene-like layer (Khalil et al 2017). The absence of any other peaks in the XRD patterns of the BAC materials indicated the absence of any other mineral contaminates in the BAC materials, which confirmed by presence of low ash ratios (as indicated by DTG results, above).

Further inspection of the patterns reveals that the intensity of the observed two diffraction peaks, were increased with increasing of pyrolysis temperature. This indicates enhancement of the crystallization process into graphite micro-crystallites, which was proceeded on the expense of successive detachment of surface functional groups (Liou 2010; Shi et al. 2016) as indicated above by FTIR spectra.

Raman spectroscopy

Raman spectra of activated carbon and other carbon systems show only a few prominent features, typically, a couple of very intense bands in the 1000–2000 cm^{-1} region and few other second-order modulations (Ferrari 2007). The peculiar dispersion of the π electrons in graphene layers is the fundamental reason why Raman spectroscopy in carbons is always resonant. Figure 3b shows Raman scattering for BAC500 material as representative. Two scattered bands centered around 1595 and 1355 cm^{-1} were observed which related to the graphitic (*G*) and disordered carbon structure (*D*). The *G* signal is attributed the E_{2g} Raman active mode of C–C stretching, whereas the *D* signal is resulted from the A_{1g} Raman mode (Wang et al. 2008). The signal intensity ratio was found to be ($R = I_D/I_G = 1.04$), which satisfies the requirement ($I_D/I_G = 0.86$–1.20) for representing high crystallization degree of graphitic carbon.

Surface textures and morphology

N_2 adsorption/desorption isotherms of BAC400, BAC500 and BAC600 are shown in Fig. 4a. The isotherms were classified as Type IV of isotherms with a hysteresis loop of H4 type, in the range of $P/P_o = 0.42$–0.99. N_2 adsorption volume, V_{N2}, was largely developed on going from BAC400 to BAC500 then decreased on going to BAC600. However, the departure of the desorption branch from the adsorption one largely increased in the direction BAC400 >> BAC500 > BAC600. Surface area, S_{BET}, values amounting to 1762, 2046 and 1925 (m^2/g), were obtained for the materials activated at 400, 500 and 600, respectively, see Table 3. The *t*-plot analysis showed the presence of microporosity as super-micropores (in the range of 1.0–2.0 nm). Further analysis of the specific surface areas into microporosity, S_{mic}, and mesoporosity, S_{meso}, reveals that S_{mic} values were 423, 488 and 317 m^2/g, whereas S_{meso} values were 1339, 1558, 1608 for the materials activated at BAC400, BAC500

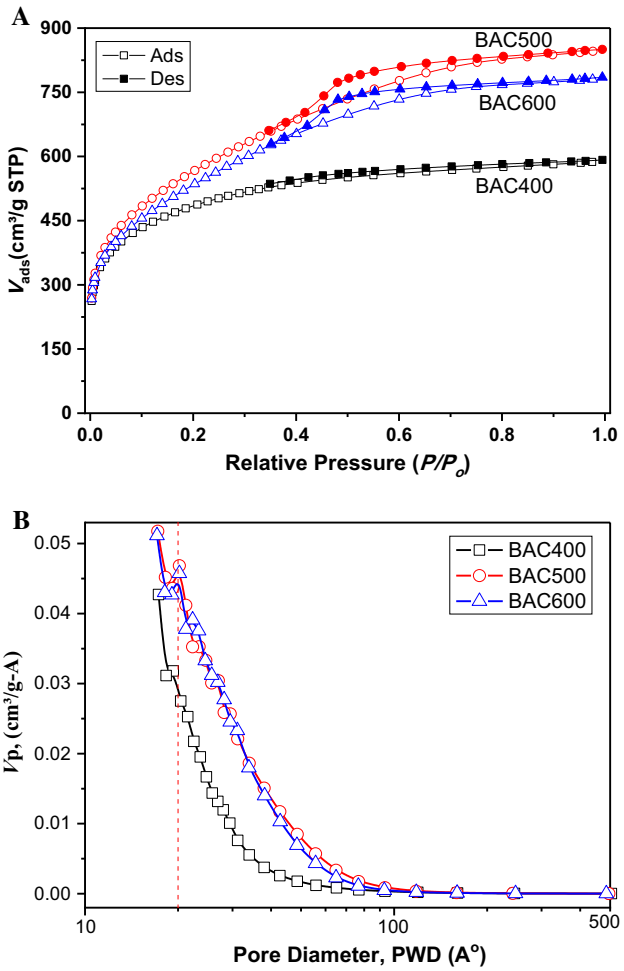

Fig. 4 Nitrogen adsorption–desorption isotherms (**a**) and pore size distributions, PSD (**b**) for BAC400, BAC500 and BAC600 materials

and BAC600. The increasing of S_{BET} value on going from ACB400 to ACB500 can be explained in terms of the release of some more volatile matters during the activation process at 500 °C, which led to creation of more micro porosity. However, the observed decrease in the S_{BET} value on going further to ACB600 was explained in terms of widening of the already formed pores via the release of further amount of volatile matters during the activation process at 600 °C. The analysis of S_{BET} into S_{mic} and S_{meso} was very important, because the adsorption capacity of phenol was related to S_{meso} rather than S_{BET}, as shown below.

To gain information about the distribution of mesoporosity, pore size distribution, PSD, plots were obtained based on the N_2 adsorption branch of isotherm by BJH method. The results are displayed in Fig. 4b, which reveals the development of small size mesoporosity < 6.0 nm and commences towards super-micropores (2.0–1.0 nm). The development of mesoporosity was increased with increasing of the activation temperatures (Zhu et al. 2016).

Table 3 Surface area, porosity and other textural characteristics of the formed BAC400, BAC500 and BAC600 materials

Sample	S_{BET} (m^2/g)	S_{meso} (m^2/g)	S_{mic} (m^2/g)	V_T (cm^3/g)	W_p $4V_T/S_{BET}$ (A°)	W_p BJH (A°)	Q_{max} (mg/g)	Q_{max} (mmol/g)	$\omega_{ph} = S_{BET}/Q_{max}N$ (nm^2)
BAC400	1762	1339	423	0.905	20.5	20.5	166.9	1.773	1.595
BAC500	2046	1558	488	1.303	25.5	29.6	181.1	1.924	1.706
BAC600	1925	1608	317	1.203	25.0	28.5	185.2	1.968	1.570

$\omega_{ph} = S_{BET}/Q_{max\_}N$

SEM micrographs for the raw material as well as the BAC materials are shown in Fig. 5a–d. The micrographs showed that the surface of the raw material was even, smooth and free from cracks, as shown in Fig. 5a, whereas the BAC materials showed successive crumbling with the formation of uneven discontinuous surfaces including cavities and voids that increased on going from BAC400 to BAC500 to BAC600, as shown in Fig. 5b–d, respectively. The indicated voids and cavities were resulted through the activation process by $ZnCl_2$ (Pezoti et al. 2014). It should be noted here that the effective nanopores responsible for the adsorption process are far smaller than the detecting limits of the employed microscope.

Phenol adsorption from solutions

Adsorption performances

Phenol adsorption on the formed BAC materials was initially monitored at different phenol concentration for successive time intervals up to 24 h. Results obtained for phenol adsorption on BAC600, as a representative, are displayed in Fig. 6. The results showed that the adsorption was very fast in the initial period (0–5 h) and then stayed almost constant up to 24 h. Adsorption of phenol was stable in the pH range 6.0–7.0 and decreased above and below this range. The pH values of the adsorption solution were amounted to 6.3 (±0.2) throughout the adsorption experiments. No significant changes were observed upon the addition of BAC

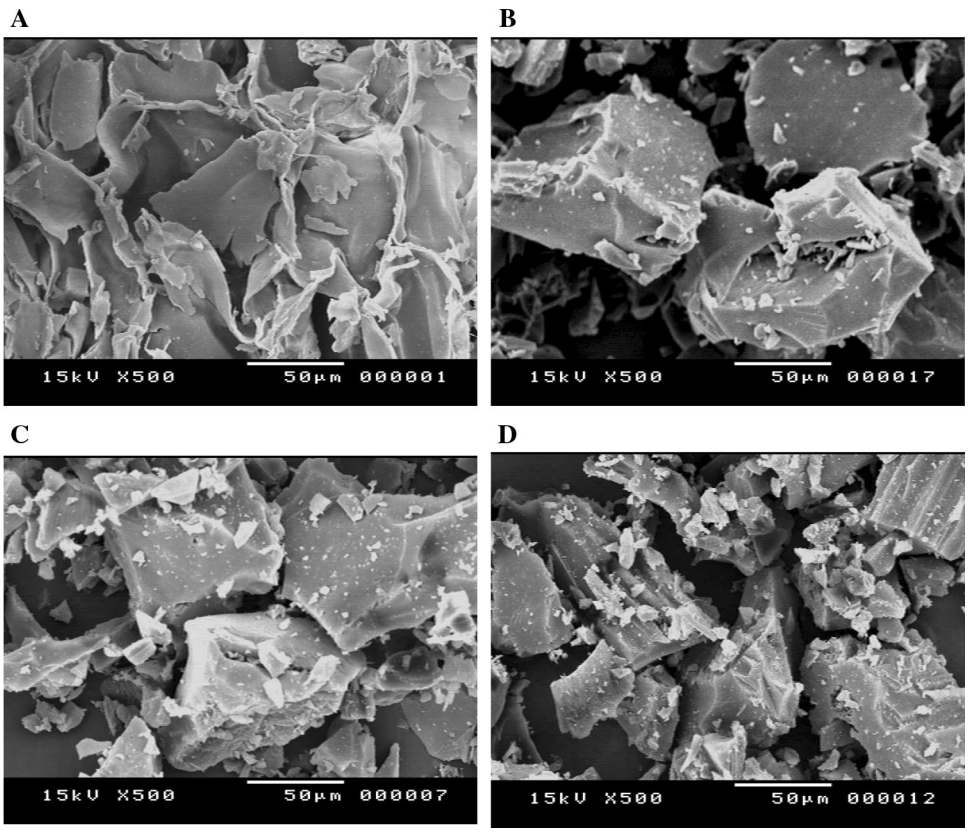

Fig. 5 SEM images for the raw sugarcane bagasse residue (**a**), BAC410 (**b**), BAC510 (**c**) and BAC610 (**d**) materials

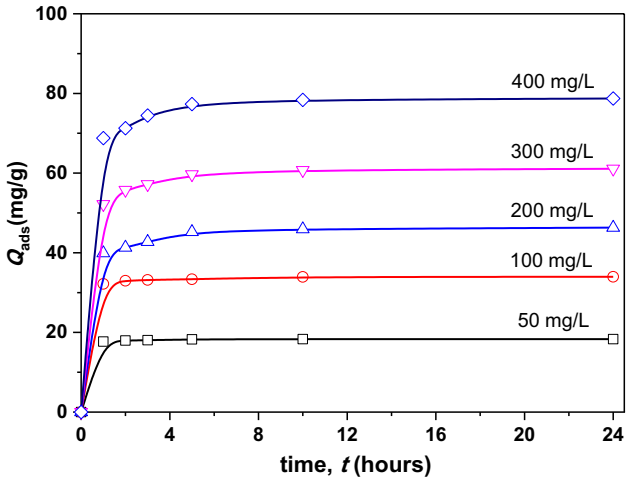

Fig. 6 The adsorption of phenol adsorption on BAC600 at different phenol concentration for successive time intervals at 25 (± 1) °C

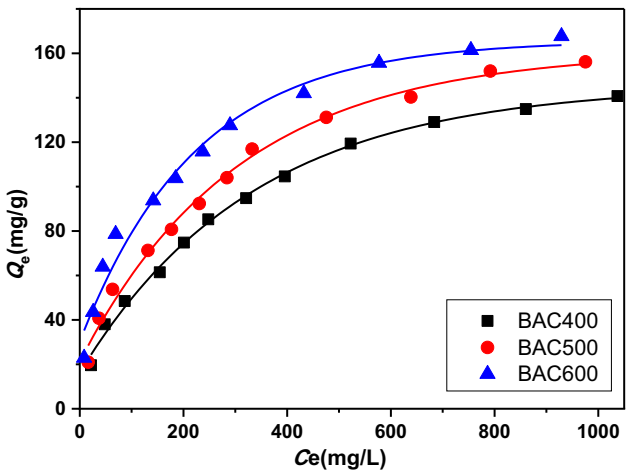

Fig. 7 The adsorption isotherms of phenol on BAC400, BAC500 and BAC600 materials at 25 (± 1) °C

materials to the phenol solutions, or during the adsorption course. This indicated that the BAC adsorbent materials contain no strong acid/base groups and/or impurities cable of *p*H modification. Therefore, the present study was focused on adsorption from neutral (unbuffered) solutions.

The adsorption isotherms of phenol at 25 (± 1 °C were measured on BAC400, BAC500 and BAC600. The adsorption isotherm provides the most essential information about the distribution of the adsorptive molecules between the liquid phase and the solid adsorbent. Typical isotherms are plotted in Fig. 7, which showed that the amount of adsorption, q_e, at a given equilibrium concentration, C_e, was increased in the order ACB400 < ACB500 < ACB600. According to the classification of adsorption isotherms of solutes from aqueous solutions proposed by Giles et al. (1974a, b) the isotherms can be classified to the Langmuir class (*L*) with subgroup (2), which relate to the plateau behavior at higher concentrations. Generally, the (*L*) class assumes that the aromatic ring adsorbs parallel to the surface and satisfies the Langmuir model assumption that no strong competition exists between the adsorbate and the solvent to occupy the adsorption sites. The molecular area available for one adsorbate molecule, $\omega_{ph} = S_{BET}/Q_{max}\_N$, are calculated as shown in Table 3. The high value of ω_{ph} (1.595, 1.706 and 1.570 nm^2 for BAC400, BAC400 and BAC400, respectively) suggests competition with water molecules.

Chemical nature of the BAC surface is the most essential factor that determines its adsorption properties. Typical chemical structure of the formed BAC surfaces is shown in Fig. 2a. To gain information about the participation of the surface functional group in the phenol adsorption process, FTIR spectra of the adsorbents before and after adsorption were investigated. Figure 2b shows FTIR spectra for BAC400 before and after phenol adsorption along with the FTIR spectra for phenol (solid phase). Comparison showed that phenol adsorption was clearly affected the 1690 and 1150 cm^{-1} bands, assigned to ν (C=O) carbonyl and ν (C–O–C), respectively. This indicates serious participation of these functional groups in the adsorption process of phenol on BAC via a ''donor–acceptor complex'' mechanism. This involves carbonyl surface-oxygen groups acting as electron donor, and the aromatic ring of the adsorbed molecules acting as acceptor (Mattson et al. 1969).

Adsorption isotherms models

The isotherms were examined with a group of two parameters isotherm models (Rangabhashiyam et al. 2014) with different assumptions to understand and optimize the adsorption process. Thus, four isotherm models, which frequently employed for phenol adsorption on BAC materials, were considered in the present study, namely the Langmuir isotherm (normally fits with ACs with homogeneous surfaces) (Langmuir 1918); the Freundlich isotherm (normally fits with ACs containing a high surface heterogeneity) (Freundlich 1909); the Dubinin–Radushkevich (D–R) isotherm (assume no homogeneous neither surface nor constant adsorption potential) (Dubinin and Radushkevich 1947); as well as the Temkin and Phyzev (Temkin and Phyzev 1940) models were examined. Table 4 summarizes the linear form equations as well as the different variables and parameters of each model.

The parameters obtained by application of each model are cited in Table S1. The correlation coefficient (r^2) was employed as criteria to estimate the fitting of each model with the experimental data. The adsorption isotherm fitting of the experimental data according to each model were constructed. It was clear from the fitting results that the

Table 4 The linear form equations and the different controlling parameters for each of the employed isotherm models

Models	Equation	Parameters
Langmuir isotherm (Langmuir 1918)	$\frac{C_e}{q_e} = \frac{1}{q_{max}K_L} + \frac{1}{q_{max}}C_e$	C_e = the equilibrium concentration (mg/L), q_e = the equilibrium adsorption capacity (mg/g), q_{max} = the maximum adsorption capacity (mg/g), and K_L is the Langmuir constant (*l*/mg). R_L = the separation factor = $1/(1+K_LC_0)$
Freundlich isotherm (Freundlich 1909)	$\log q_e = \log K_F + (1/n)\log C_e$	K_F = Freundlich adsorption constant (mg/g) $(mg/L)^{1/n}$ $1/n$ = the adsorption intensity parameter ($1/n$), with a value b
Dubinin–Radushkevich (D–R) (Dubinin and Radushkevich 1947)	$\ln q_e = \ln q_s - \beta\varepsilon^2$	q_s = the theoretical monolayer saturation capacity (mg/g), β = the D–K model constant ($mol^2\ kJ^{-2}$), ε = the Polanyi adsorption potential, $\varepsilon = RT\ln(1+1/C_e)$, E = the mean free energy of sorption (kJ/mol) $E = E = 1/\frac{1}{\sqrt{2\beta}}$
Temkin and Phyzev isotherm (Temkin and Phyzev 1940)	$q_e = B\ln K_T + B\ln C_e$	$B = RT/b_T$ is related to the heat of adsorption (*l*/*g*), and K_T = the Temkin isotherm constant, dimensionless

results fitted better with the Langmuir model in comparison to the Freundlich, Dubinin–Radushkevich (D–R), and Temkin and Phyzev isotherm models. The plots for the most promising fitting models, the Langmuir and the Freundlich models are presented in Fig. 8.

In lights of the applicability of the Langmuir isotherm model to the present phenol adsorption process, the separation factor (R_L), which expressed as a dimension less equilibrium parameter and given as: $R_L = 1/(1+K_LC_o)$, see Table 4.

The value of *R*L gives probability of the adsorption isotherm to be favorable, unfavorable, irreversible or Linear based on the value of *RL*, as $(0<RL<1)$, $(RL>1)$, $(RL=0)$ or $(RL=1)$, respectively (Hameed and Rahman 2008).

The present investigation indicated that *RL* values were amounted to 0.1172, 0.0991 and 0.0611 for BAC400, BAC500 and BAC600, respectively. Accordingly, the favorability of phenol adsorption on the prepared BACs materials was suggested.

Adsorption capacity, Q_{max} (mg/g), amounting to 166.9, 181.1, and 185.2 were calculated for BAC400, BAC500 and BAC600, respectively. A comparison between the adsorption capacity of phenol on the present BAC materials with other ACs and/or other type of adsorbent materials, are summarized in Table 5. Accordingly, the present BACs adsorbent showed better adsorption capacity than many commercial and recently investigated AC materials (Kumar and Jena 2016; Srivastava et al. 2006) and comparable with other well-known ACs (Okolo et al. 2000) materials.

Adsorption kinetics

The adsorption of phenol on the prepared BAC materials was investigated by the pseudo-first-order and pseudo-second-order kinetic models. The linear form of pseudo-first-order

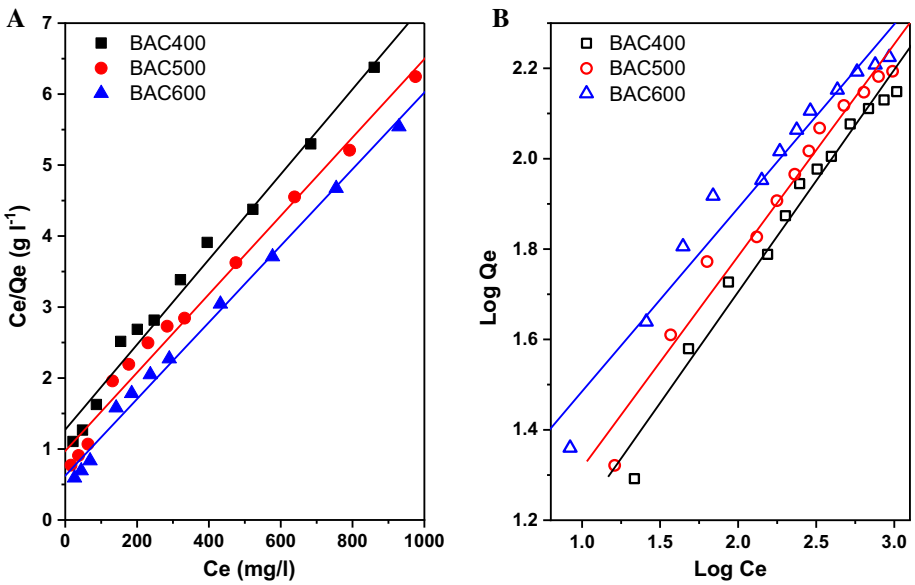

Fig. 8 The adsorption isotherm empirical data fitting to the linear form of Langmuir (**a**) and Freundlich (**b**) isotherm model

Table 5 Comparison of adsorption capacities of phenol from aqueous solutions on various activated carbon materials

Adsorbent	Adsorption capacity *qe* (mg/g)	Reference
Sugarcane bagasse residue	185.2	This work
Sugarcane bagasse fly ash	23.8	Srivastava et al. (2006)
Pine fruit shell biochar	27	Mohammed et al. (2018)
Na–Y zeolites	75.28	Okolo et al (2000)
Activated carbon from Fox nutshell	75.4	Kumar and Jena (2016)
Wood derived activated carbon	128.9	Ge et al. (2020)
Rattan sawdust-based activated carbon	149.3	Hameed and Rahman (2008)
Activated carbon	185	Khraisheh et al. (2020)
Physiochemical-activated coconut shell	205.8	Zhu et al. (2016)
Sugarcane bagasse	210.8	Greish et al. (2021)
Activated carbon (AC) prepared from palm kernel shell (PKS)	291.7	Boontham et al. (2020)

is illustrated according to the following equation (Shi et al. 2016):

$$\ln\left(q_e - q_t\right) = \ln q_e - k_1 t \tag{2}$$

where q_e and q_t are the amounts of phenol adsorbed (mg/g) at equilibrium and time t, respectively, and k_1 is the rate constant of adsorption (h^{-1}).

The pseudo-second-order model can be given in the following form (Ferrari 2007):

$$\frac{t}{q_t} = \frac{1}{k_2 q_e^2} + \frac{1}{q_e} t \tag{3}$$

where k_2 (g/mg-h) is the rate constant of the second-order equation. A plot of t/q versus time (t) will give a straight line with a slope of $1/q_e$.

Fitting of the empirical date with the above kinetic equations is shown in Fig. 9a, b. The obtained kinetic parameters are summarized in Table S2. It is obvious that the correlation coefficient, r^2, values obtained from the pseudo-second-order were very close to unity.

Adsorption thermodynamics

The influence of temperature on the adsorption capacity of phenol on to BACs materials was explored over the range of at 298–318 K. Thus, the adsorption capacity of phenol was decreased with increasing of temperature. The main thermodynamic parameters such as a change in Gibbs free energy ($\Delta G°$), change in enthalpy ($\Delta H°$) and change in entropy ($\Delta S°$) were evaluated according to the following equations:

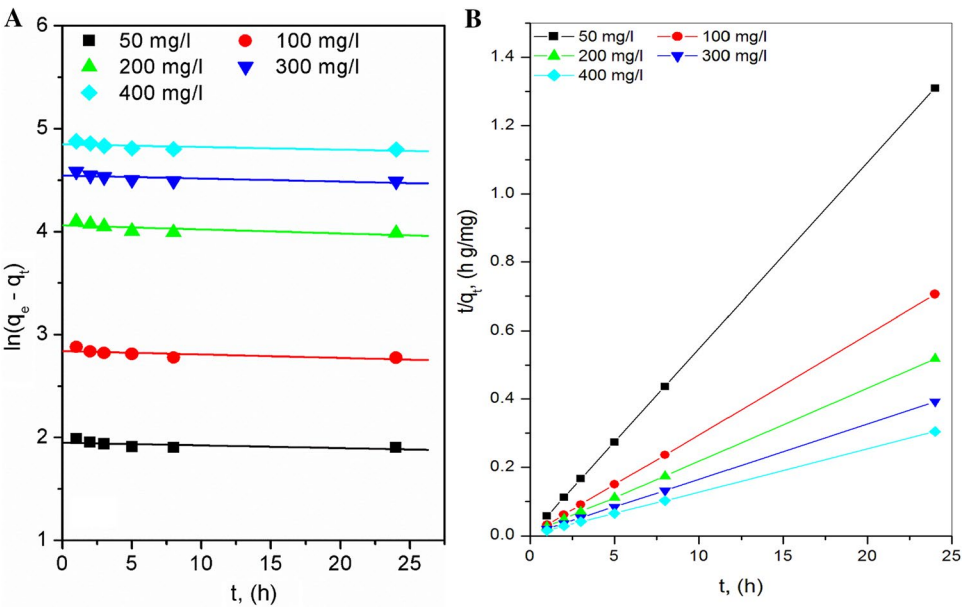

Fig. 9 The empirical data fitting to **a** pseudo-first-order and **b** pseudo-second-order kinetics of phenol adsorption at 25 (± 1) °C

$$\Delta G^{\circ} = -RT \ln K_{\mathrm{L}} \tag{4}$$

$$\ln K_L = \frac{\Delta S^{\circ}}{R} - \frac{\Delta H^{\circ}}{RT} \tag{5}$$

where R is the universal gas constant, 8.314 J/mol K, T (K) is the absolute solution temperature, and K_{L} (L/g) is the Langmuir isotherm constant. The values of $\Delta G°$, $\Delta H°$ and $\Delta S°$ were determined and are cited in Table S3. Typical values of $\Delta G°$ (14.66–15.01 J/mol K) indicating physical adsorption were obtained in the present study. The numerical values of $\Delta H°$ and $\Delta S°$ were generated from the linear relation of ln K_{L} versus $1/T$. The obtained values of $\Delta H°$ and $\Delta S°$ were − 9.7 kJ/mol and + 16.8 kJ/mol/K, respectively. The negative values of the enthalpy change $\Delta H°$ indicate that the phenol adsorption process onto the BACs surface was exothermic in nature and temperature increasing is not favorable for adsorption of phenol. While, the positive value of $\Delta S°$ of phenol adsorption shows the decreased randomness from the thermodynamic point of view. Moreover, the absolute value of $\Delta H^{\circ}_{\mathrm{ads}}$ is in the range of ≤ 40 kJ/mol, which confirms that adsorption of phenol on BACs is consistent with a mechanism that involves physical adsorption.

Comparative adsorption of phenol, di- and tri-hydroxyl phenols

A comparative study for the adsorption of phenol (a monohydroxyl phenol) as well as resorcinol and pyrogallol (as a *di*- and *tri*-hydroxyl phenols) was carried out in order to understand the nature of the adsorption process and extend the applicability of the BAC materials. Typical adsorption isotherms obtained with phenol, resorcinol and pyrogallol on BAC400 are presented in Fig. 10a, b where the isotherms were constructed in terms of mass unit and molar mass unite, respectively. Some physical properties of phenol, resorcinol and pyrogallol are shown in Table S4.

The isotherms of phenol, resorcinol and pyrogallol showed an identical behavior from a qualitative point of view. The isotherms can be classified as (L2) class of adsorption isotherm, according to the Giles classification scheme (Giles et al. 1974a, b).

Quantitatively, the comparative adsorption isotherms in mass unit, as shown in Fig. 10a, Q_{eq} (mg/g) against C_{eq} (mg/L), showed that the adsorption capacity increased in the order of phenol < resorcinol < pyrogallol, which is the same order of increasing: of the number of hydroxyl groups (1, 2 and 3), molecular mass (94.11, 110.10 and 126.11 g/mol), and melting points (40.5, 110 and 131 °C), respectively. This trend indicates that the adsorption of phenolic compounds on BAC adsorbents increased with

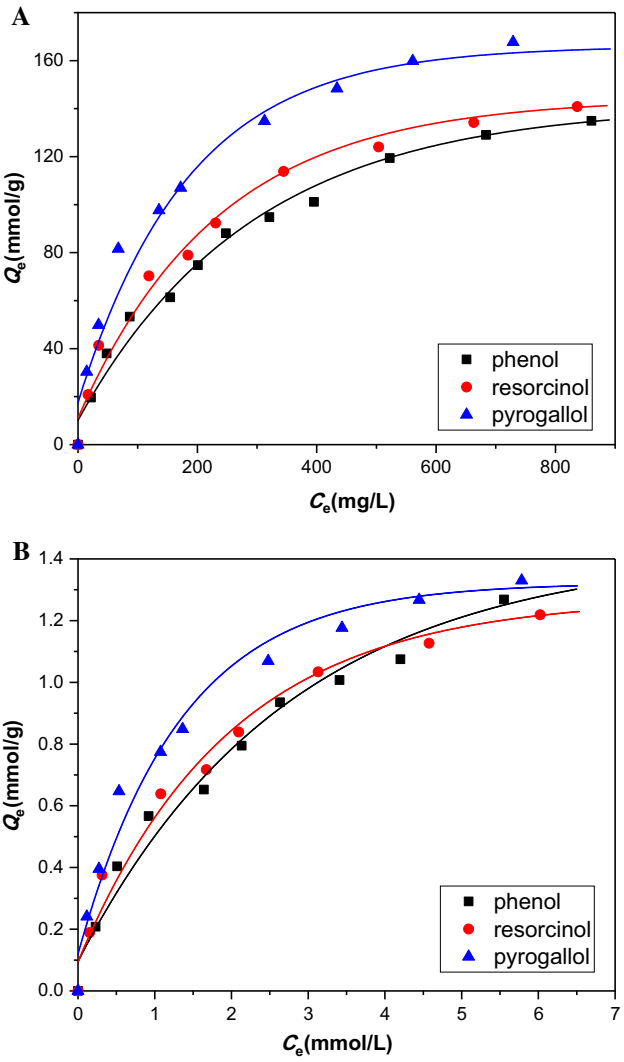

Fig. 10 Typical adsorption isotherms in mass unit (**a**) and in molar mass unit (**b**) for phenol, resorcinol and pyrogallol adsorbed on ACB600

the increasing of intermolecular bonding forces all over the examined concentration range up to 1000 mg/L.

The same trend was also observed for the isotherms constructed in molar mass unit, Q_{eq} (mmol/g), against molar concentrations C_{eq} (mmol/L), as shown in Fig. 10b. However at relatively higher molar concentrations (> 4.5 mmol/L) the order of molar adsorption capacity was in the order of resorcinol < phenol < pyrogallol, which is the typical order of solubility decrease (110, 80.2 and 40 g/100 mL) for resorcinol, phenol and pyrogallol, respectively.

Similar comparative adsorption isotherms of substituted phenols have been investigated to gain information about the adsorption behavior in other adsorption systems. For instance, adsorption of 1-naphthol and naphthalene on biochar has been investigated and it has been found that adsorption capacity of 1-naphthol significantly larger

than naphthalene due to the additional specific interactions (Chen and Chen 2009). Moreover, adsorption of some substituted phenols on other AC materials has been investigated and it has been found that the uptake was changed in the order of lowering of solubility in water as: 2-chlorophenol > 4-chlorophenol > phenol (Strachowski, and Bystrzejewski 2015). These examples support the present justification based on the comparative adsorption phenol, resorcinol and pyrogallol.

Conclusion

The above formed BACs materials showed good adsorption capacities toward adsorptive removal of phenolic compounds as compared with other recently investigated materials. The equilibrium data were better represented by Langmuir adsorption model and pseudo-second-order kinetics. The results confirm presence of mutual adsorbent/adsorbate interaction through the following justified mechanisms:

1. electron donor–acceptor interactions: Surface functional groups on the surface of the BAC materials were modified over increasing of the activation temperature from carboxyl into carbonyl. This situation led to a ''donor–acceptor'' mechanism in which, the carbonyl surface-oxygen groups acting as electron donor, and the aromatic ring of the adsorbate molecules acting as acceptor. This interaction led to increasing of the adsorption capacity as BAC400 < BAC500 < BAC600.
2. dispersion interaction between π-electrons of the graphitic structures and the aromatic phenolic ring: Comparative adsorption studies of substituted phenols indicates that adsorption of phenolic compounds on BAC adsorbents was increased as phenol < resorcinol < pyrogallol. That is with increasing of intramolecular bonding strength of the phenolic structure with graphitic layers of BAC.

Therefore, the present work emphasized that BAC showed many interesting characteristics that led to efficient adsorption of phenols via tuned adsorbent/adsorbate interaction all over the examined phenolic concentration range. This situation was accomplished by the improved textural properties of the nanographitic structure.

Supplementary Information The online version contains supplementary material available at https://doi.org/10.1007/s13762-021-03382-3.

Acknowledgements The authors are greatly acknowledged the fund received during this project sponsored by STDF (Egypt). Grant number: TC Water ID 20709, PI: Prof. Kamal M.S. Khalil.

References

Abo ELNaga AO, El Saied M, Shaban SA, El Kady FY (2019) Fast removal of diclofenac sodium from aqueous solution using sugar cane bagasse-derived activated carbon. J Mol Liquids 285:9–19. https://doi.org/10.1016/j.molliq.2019.04.062

Açıkyıldız M, Gürses A, Karaca S (2014) Preparation and characterization of activated carbon from plant wastes with chemical activation. Microporous Mesoporous Mater 198:45–49

Adinaveen T, Kennedy LJ, Vijaya JJ, Sekaran G (2013) Studies on structural, morphological, electrical and electrochemical properties of activated carbon prepared from sugarcane bagasse. J Ind Eng Chem 19:1470–1476. https://doi.org/10.1016/j.jiec.2013.01.010

Al-Malack MH, Dauda M (2017) Competitive adsorption of cadmium and phenol on activated carbon produced from municipal sludge. J Environ Chem Eng 5:2718–2729

Angin D (2014) Production and characterization of activated carbon from sour cherry stones by zinc chloride. Fuel 115:804–811

Bernal V, Giraldo L, Moreno-Piraján JC (2020) Adsorption of pharmaceutical aromatic pollutants on heat-treated activated carbons: effect of carbonaceous structure and the adsorbent-adsorbate interactions. ACS Omega 5:15247–15256. https://doi.org/10.1021/acsomega.0c01288

Boontham W, Habaki H, Egashira R (2020) Removal of phenol from oil mill effluent using activated carbon prepared from Kernel Shell in Thailand's Palm Industry. J Chem Eng Jpn 53:682–688

Brunauer S, Emmett PH, Teller E (1938) Adsorption of gases in multimolecular layers. Am Chem Soc 60(1):309–319

Cai Y, Liu L, Tian H, Yang Z, Luo X (2019) Adsorption and desorption performance and mechanism of tetracycline hydrochloride by activated carbon-based adsorbents derived from sugar cane bagasse activated with $ZnCl_2$. Molecules 24:4534. https://doi.org/10.3390/molecules24244534

Chai X, He H, Fan H, Kang X, Song X (2019) A hydrothermal-carbonization process for simultaneously production of sugars, graphene quantum dots, and porous carbon from sugarcane bagasse. Bioresour Technol 282:142–147. https://doi.org/10.1016/j.biortech.2019.02.126

Chen B, Chen Z (2009) Sorption of naphthalene and 1-naphthol by biochars of orange peels with different pyrolytic temperatures. Chemosphere 76:127–133. https://doi.org/10.1016/j.chemosphere.2009.02.004

Coates J (2000) Interpretation of infrared spectra, a practical approach. Encycl Anal Chem. https://doi.org/10.1002/9780470027318

Congsomjit D, Areeprasert C (2020) Hydrochar-derived activated carbon from sugar cane bagasse employing hydrothermal carbonization and steam activation for syrup decolorization. Biomass Convers Biorefinery. https://doi.org/10.1007/s13399-020-00635-y

Dabrowski A, Podkoscielny P, Hubicki Z, Barczak M (2005) Adsorption of phenolic compounds by activated carbon-acritical review. Chemosphere 58(8):1049–1070

Derylo-marczewska A, Buczek B, Swiatkowski A (2011) Effect of oxygen surface groups on adsorption of benzene derivatives from aqueous solutions onto active carbon samples. Appl Surf Sci 257:9466–9472. https://doi.org/10.1016/j.apsusc.2011.06.036

Dubinin MM, Radushkevich LV (1947) Equation of the characteristic curve of activated charcoal. Proc Acad Sci USSR Phys Chem Sect 55:331

Eslami A, Borghei SM, Rashidi A, Takdastan A (2018) Preparation of activated carbon dots from sugarcane bagasse for naphthalene removal from aqueous solutions. Sep Sci Technol 53:2536–2549. https://doi.org/10.1080/01496395.2018.1462832

Ferrari AC (2007) Raman spectroscopy of graphene and graphite: disorder, electron–phonon coupling, doping and nonadiabatic effects. Solid State Commun 143:47–57

Freundlich H (1909) einedarstellung der chemie der kolloide und verwantergebiete. Kapillarchemie. AcademisheBibliotek, Leipzig

Ge X, Wu Z, Manzoli M, Wu Z, Cravotto G (2020) Feasibility and the mechanism of desorption of phenolic compounds from activated carbons. Ind Eng Chem Res 59:12223–12231

Giles CH, D'Silva AP, Easton IA (1974a) A general treatment and classification of the solute adsorption isotherm, II. Experimental interpretation. J Colloid Interface Sci 47:766–778

Giles CH, Smith D, Huitson A (1974b) A general treatment and classification of the solute adsorption isotherm. I. Theoretical. J Colloid Interface Sci 47:755–765

Girods P, Dufour A, Fierro V, Rogaume Y, Rogaume C, Zoulalian A, Celzard A (2009) Activated carbons prepared from wood particleboard wastes: characterisation and phenol adsorption capacities. J Hazard Mater 166:491–501

Gonçalves R, Martins C, Mendes N, Farias L, Sousa D, Cristina R et al (2014) Preparation of activated carbons from cocoa shells and siriguela seeds using H 3 PO 4 and ZnCL 2 as activating agents for BSA and α -lactalbumin adsorption. Fuel Process Technol 126(2014):476–486. https://doi.org/10.1016/j.fuproc.2014.06.001

Greish AA, Sokolovskiy PV, Finashina ED, Kustov LM, Vezentsev AI, Chien ND (2021) Adsorption of phenol and 2,4-dichlorophenol on carbon-containing sorbent produced from sugar cane bagasse. Mendeleev Commun 31(1):121–122. https://doi.org/10.1016/j.mencom.2021.01.038

Gundogdu A, Duran C, Senturk HB, Soylak M, Ozdes D, Serencam H, Imamoglu M (2012) Adsorption of phenol from aqueous solution on a low-cost activated carbon produced from tea industry waste: equilibrium, kinetic, and thermodynamic study. J Chem Eng Data 57:2733–2743. https://doi.org/10.1021/je300597u

Halsey G (1948) Physical adsorption on non-uniform surfaces. J Chem Phys 16(10):931

Hameed BH, Rahman AA (2008) Removal of phenol from aqueous solutions by adsorption onto activated carbon prepared from biomass material. J Hazard Mater 160:576–581

Hazzaa R, Hussein M (2015) Adsorption of cationic dye from aqueous solution onto activated carbon prepared from olive stones. Environ Technol Innov 4:36–51

Karri RR, Sahub JN, Jayakumar NS (2017a) Optimal isotherm parameters for phenol adsorption from aqueous solutions onto coconut shell based activated carbon: error analysis of linear and nonlinear methods. J Taiwan Inst Chem Eng 80(2017):472–487

Karri RR, Jayakumar NS, Sahu JN (2017b) Modelling of fluidised-bed reactor by differential evolution optimization for phenol removal using coconut shells based activated carbon. J Mol Liq 231:249–262

Karri RR, Sahu JN, Meikap BC (2020) Improving efficacy of Cr (VI) adsorption process on sustainable adsorbent derived from waste biomass (sugarcane bagasse) with help of ant colony optimization. Ind Crops Product 143:111927 https://doi.org/10.1016/j.indcrop.2019.111927

Khalil KMS, Allam OAS, Khairy M, Mohamed KMH, Elkhatib RM, Hamed MA (2017) High surface area nanostructured activated carbons derived from sustainable sorghum stalk. J Mol Liq 247:386–396

Khenniche L, Benissad-Aissani F (2010) Adsorptive removal of phenol by coffee residue activated carbon and commercial activated carbon: equilibrium, kinetics, and thermodynamics. J Chem Eng Data 55(11):4677–4686. https://doi.org/10.1021/je100302e

Khraisheh M, Al-Ghouti MA, AlMomani F (2020) *P. putida* as biosorbent for the remediation of cobalt and phenol from industrial waste waste waters. Environ Technol Innov 20:101148. https://doi.org/10.1016/j.eti.2020.101148

Kumar A, Jena MH (2016) Removal of methylene blue and phenol onto prepared activated carbon from Fox nutshell by chemical activation in batch and fixed-bed column. J Clean Prod 137:1246–1259

Langmuir I (1918) The adsorption of gases on plane surface of glass, mica and olatinum. J Am Chem Soc 40:1361–1403. https://doi.org/10.1021/ja02242a004

Liou T (2010) Development of mesoporous structure and high adsorption capacity of biomass-based activated carbon by phosphoric acid and zinc chloride activation. Chem Eng J 158:129–142. https://doi.org/10.1016/j.cej.2009.12.016

Long S, Du Q, Wang S, Tang P, Li D (2019) Graphene two-dimensional crystal prepared from cellulose two-dimensional crystal hydrolysed from sustainable biomass sugarcane bagasse. J Clean Prod 241:118209. https://doi.org/10.1016/j.jclepro.2019.118209

Lorenc-Grabowska E, Diez MA, Gryglewicz G (2016) Influence of pore size distribution on the adsorption of phenol on PET-based activated carbons. J Colloid Interface Sci 469:205–212

Luo X (2019) Cr (VI) adsorption performance and mechanism of an effective activated carbon prepared from bagasse with a one-step pyrolysis and $ZnCl_2$ activation method. Cellulose 26:4921–4934. https://doi.org/10.1007/s10570-019-02418-9

Magne P, Walker PL Jr (1986) Phenol adsorption on activated carbons: application to the regeneration of activated carbons polluted with phenol. Carbon 24(1986):101–107

Mattson JS, Mark HB Jr, Malbin MD, Weber WJ Jr, Crittenden JC (1969) Surface chemistry of active carbon: specific adsorption of phenols. J Colloid Interface Sci 31:116–130

Michailof C, Stavropoulos GG, Panayiotou C (2008) Enhanced adsorption of phenolic compounds, commonly encountered in olive mill wastewaters, on olive husk derived activated carbons. Bioresour Technol 99(14):6400–6408

Mohammed NAS, Abu-Zurayk RA, Hamadneh I, Al-Dujaili AH (2018) Phenol adsorption on biochar prepared from the pine fruit shells: equilibrium, kinetic and thermodynamics studies. J Environ Manag 226:377–385

Okolo B, Park C, Keane MA (2000) Interaction of phenol and chlorophenols with activated carbon and synthetic zeolites in aqueous media. J Colloid Interface Sci 226:308. https://doi.org/10.1006/jcis.2000.6796

Pezoti O, Cazetta AL, Souza IP, Bedin KC, Martins AC, Silva TL, Almeida VC (2014) Adsorption studies of methylene blue onto ZnCl2-activated carbon produced from buriti shells (*Mauritia flexuosa* L.). Ind Eng Chem 20:4401–4407

Priya DS, Sureshkumar MV (2020) Synthesis of *Borassus flabellifer* fruit husk activated carbon flter for phenol removal from wastewater. Int J Environ Sci Technol 17:829–842. https://doi.org/10.1007/s13762-019-02325-3

Rambabu N, Rao BVSK, Surisetty VR, Das U, Dalai AK (2014) Production, characterization, and evaluation of activated carbons from de-oiled canola meal for environmental applications. Ind Crops Prod 65:572–581

Rangabhashiyam S, Anu N, Giri Nandagopal MS, Selvaraju N (2014) Relevance of isotherm models in biosorption of pollutants by agricultural, byproducts. J Environ Chem Eng 2:398–414

Shi J, Wang Y, Du W, Hou Z (2016) Synthesis of graphene encapsulated Fe3C in carbon nanotubes from biomass and its catalysis application. Carbon 99:330–337

Sing KSW, Everett DH, Haul RAW, Moscou L, Pierotti RA, Rouquerol J, Siemieniewska T (1985) Reporting physisorption data for gas/solid systems with special reference to the determination of surface area and porosity (Recommendations 1984). Pure Appl Chem 57(4):603–619

Solís-fuentes JA, Galán-méndez F, Hernández-medel MR, García-gómez RS, Bernal-gonzález M, Mendoza-pérez S et al (2019) Effectiveness of bagasse activated carbon in raw cane juice

clarification. Food Biosci 32:100437. https://doi.org/10.1016/j.fbio.2019.100437

Srivastava VC, Swamy MM, Mall I, Prasad B, Mishra I (2006) Adsorptive removal of phenol by bagasse fly ash and activated carbon: equilibrium, kinetics and thermodynamics. Colloids Surf 272:89–104

Strachowski P, Bystrzejewski M (2015) Comparative studies of sorption of phenolic compounds onto carbon-encapsulated iron nanoparticles, carbon nanotubes and activated carbon. Colloids Surf A 467:113–123. https://doi.org/10.1016/j.colsurfa.2014.11.044

Temkin MJ, Phyzev V (1940) Recent modifications to Langmuir isotherms. Acta Physiochim USSR 12:217–222

Velasco LF, Carmona RJ, Matos J, Ania CO (2014) Performance of activated carbons in consecutive phenol photooxidation cycles. Carbon 73:206–215

Villegas LGC, Mashhadi N, Chen M, Mukherjee D, Taylor KE, Biswas N (2016) A short review of techniques for phenol removal from wastewater. Curr Pollut Rep. https://doi.org/10.1007/s40726-016-0035-3

Wang Y, Su F, Wood CD, Lee JY, Zhao XS (2008) Preparation and characterization of carbon nanospheres as anode materials in lithium-ion secondary batteries. Ind Eng Chem Res 47:2294–2300

Wassie AB, Srivastava VC (2016) (2016) Chemical treatment of teff straw by sodium hydroxide, phosphoric acid and zinc chloride: adsorptive removal of chromium. Int J Environ Sci Technol 13:2415–2426. https://doi.org/10.1007/s13762-016-1080-6

Yagmur E, Turkoglu S, Banford A, Aktas Z (2017) The relative performance of microwave regenerated activated carbons on the removal of phenolic pollutants. J Clean Prod 149:1109–1117

Yang T, Lua AC (2006) Textural and chemical properties of zinc chloride activated carbons prepared from pistachio-nut shells. Mater Chem Phys 100:438–444

Yang J, Qiu K (2010) Preparation of activated carbons from walnut shells via vacuum chemical activation and their application for methylene blue removal. Chem Eng J 165:209–217

Zhu G, Deng X, Hou M, Sun K, Zhang Y, Li P, Liang F (2016) Comparative study on characterization and adsorption properties of activated carbons by phosphoric acid activation from corncob and its acid and alkaline hydrolysis residues. Fuel Process Technol 144:255–261